DE GRUYTER Adv. Opt. Techn. 2017; 6(6): 459–466

Research Article

Jan Bußmann*, Michal Odstrčil, Yusuke Teramoto and Larissa Juschkin

Ptychographic imaging with partially coherent plasma EUV sources

https://doi.org/10.1515/aot-2017-0050
Received August 7, 2017; accepted September 13, 2017; previously published online December 4, 2017

Abstract: We report on high-resolution lens-less imaging experiments based on ptychographic scanning coherent diffractive imaging (CDI) method employing compact plasma sources developed for extreme ultraviolet (EUV) lithography applications. Two kinds of discharge sources were used in our experiments: a hollow-cathode-triggered pinch plasma source operated with oxygen and for the first time a laser-assisted discharge EUV source with a liquid tin target. Ptychographic reconstructions of different samples were achieved by applying constraint relaxation to the algorithm. Our ptychography algorithms can handle low spatial coherence and broadband illumination as well as compensate for the residual background due to plasma radiation in the visible spectral range. Image resolution down to 100 nm is demonstrated even for sparse objects, and it is limited presently by the sample structure contrast and the available coherent photon flux. We could extract material properties by the reconstruction of the complex exit-wave field, gaining additional information compared to electron microscopy or CDI with longer-wavelength high harmonic laser sources. Our results show that compact plasma-based EUV light sources of only partial spatial and temporal coherence can be effectively used for lens-less imaging applications. The reported methods may be applied in combination with reflectometry and scatterometry for high-resolution EUV metrology.

***Corresponding author: Jan Bußmann,** RWTH Aachen University, Experimental Physics of Extreme Ultraviolet EUV, JARA-FIT, Aachen, Germany; and Forschungszentrum Jülich, PGI-9, JARA-FIT, Jülich, Germany, e-mail: jan.bussmann@rwth-aachen.de
Michal Odstrčil: Paul Scherrer Institute, Coherent X-ray Scattering Group, Villigen, SH, Switzerland
Yusuke Teramoto: BLV Licht- und Vakuumtechnik GmbH, Aachen, Germany
Larissa Juschkin: RWTH Aachen University, Experimental Physics of Extreme Ultraviolet EUV, JARA-FIT, Aachen, Germany; and Forschungszentrum Jülich, PGI-9, JARA-FIT, Jülich, Germany

www.degruyter.com/aot
© 2017 THOSS Media and De Gruyter

Keywords: EUV; laboratory EUV source; partial coherence; ptychography.

1 Introduction

To increase the resolution and depth of focus and improve material identification in nanometrology tools, a short illumination wavelength is desired [1]. Extreme ultraviolet (EUV) radiation covering the spectral range between 2.5 and 124 nm wavelength (10–500 eV photon energy) is a good candidate to satisfy this demand. The strong absorption of EUV radiation in all solid materials provides high contrast, as most of the element-specific L- and M-absorption edges are within this spectral range.

Sources of EUV radiation, such as free electron lasers, synchrotrons, laser high harmonic generation, and discharge- and laser-produced plasmas, differ by size, stability, coherence, and output power. Our experimental tools are based on laboratory discharge EUV sources, where light is emitted from hot and dense plasmas. These sources emit high-energy photons from 1 to 150 nm spectral range [2], covering the "water window" [3] and common absorptions edges [4].

Initially designed for projection EUV lithography, EUV light from the discharge plasma is also used nowadays for metrology purposes, for example, reflectometry [5–7], scatterometry [8], photoemission electron microscopy [9], and magnetic polarization spectroscopy [4]. Furthermore, the current applications in nanostructuring using discharge EUV sources are focused on laboratory-size interference lithography [10] as well as resist and optics defectivity studies [11].

As the strong absorption properties of materials impede the use of conventional refractive optics in the EUV range, reflective or diffractive optics must be used. Therefore, such optical systems suffer from low photon efficiency, complexity, and high cost. Lens-less imaging offers an alternative solution allowing to achieve diffraction-limited image quality without the use of complex optics.

Starting with a synchrotron X-ray experiment [12], coherent imaging and particularly ptychography [13, 14] are now well-established techniques for short-wavelength imaging [15]. Presently, experiments demonstrated a resolution of 12.5 nm using laboratory-based EUV sources for the imaging of highly scattering samples [16]. Isotropic 3D resolution of 14.6 nm has been also demonstrated at large-scale facilities [17]. To enable a more efficient use of emitted photons, polychromatic [18, 19] and broadband illumination schemes [20] were already successfully adapted for ptychographic microscopy experiments. Research groups are working on the design of industrial tools using ptychography methods for EUV mask defect inspection [21, 22], taking advantage of the simultaneous reconstruction of phase and amplitude to detect otherwise not observable defects. Coherent diffraction imaging experiments using a gas discharge EUV source of low spatial coherence have already been presented by our group [23, 24]. In this article, we report on the reconstruction of an image of a silicon nitride grid covered with a thin metal film and the determination of material properties of this film. Furthermore, the imaging of a sparse and thus less scattering sample has been demonstrated. The presented results extend ptychography to the case of not only low spatial coherence but also broadband illumination with laboratory-scale and industrially relevant plasma EUV sources.

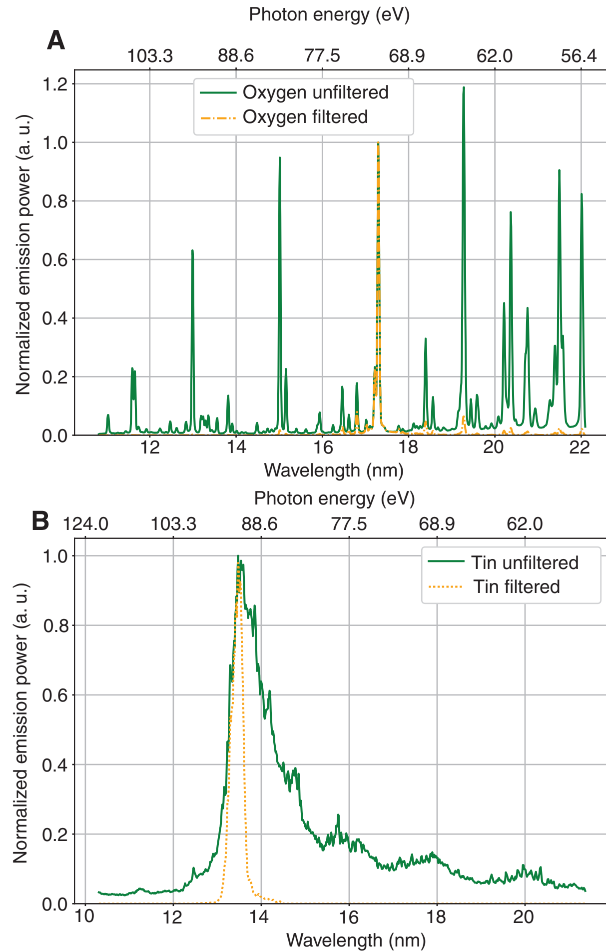

Figure 1: (A) Emission spectra before and after spectral filtering of the oxygen plasma EUV emission. In green, a typical gas discharge oxygen spectrum is shown with its sharp emission lines. The dotted orange line shows the illumination spectrum after reflection from an Si/B_4C multilayer mirror. The oxygen spectra are normalized to the emission power at 17.3 nm. Small satellite emission lines at about 16.5 nm, at 18.5 and 19.3 nm, are clearly visible even after multilayer filtering. (B) LDP tin emission with and without filtering is shown in green and orange, respectively. In contrast to oxygen, the filtered tin spectrum has a broad but smooth transition to zero without any satellite emission lines. The tin spectra are normalized to their peak value at 13.5 nm.

2 Experimental setup

The narrow bandwidth illumination experiments were performed with gas discharge plasma (GDP) sources developed at the Fraunhofer Institute for Laser Technology (ILT) [25, 26]. The sources use high-voltage discharge plasmas generating line emission spectrum (for light elements) or a quasi-continuous spectrum (for heavy elements) with peak intensity between 20 and 600 eV photon energy or 62.0 to 2.1 nm wavelength, respectively. Figure 1A shows the emission spectrum of oxygen. A reflection from a Si/B_4C Bragg mirror $[Si\ (8.04\ nm)/B_4C\ (5.36\ nm)]_{x50}$ was used to spectrally filter the light and select the intense doublet of O^{5+} at 17.3 nm (71.7 eV, Li-like oxygen, $1s^22p$-$1s^23d$ transition). Additionally, the residual oxygen in the system serves as VUV filter for emission above 30 nm wavelength. According to the CXRO X-ray database [27], under 43° grazing incidence angle of illumination, the mirror reflectivity peaks at 20% reflectivity and the bandwidth [full-width at half-maximum (FWHM)] of 3% for unpolarized 17.3 nm light. The multilayer mirror suppresses the satellite lines but does not reduce further the bandwidth of the illumination, as the doublet spectral line at 17.3 nm is much narrower than the mirror bandwidth ($\Delta\lambda/\lambda \approx 10^{-3} = 0.1\%$). Figure 1A shows also the mirror-filtered spectrum. The contributions of the satellite lines must nevertheless be included into the reconstruction process to maintain the reconstruction quality [23].

The oxygen plasma EUV emitting region has a diameter of 0.7 mm. The radial intensity distribution of Lorentzian shape transverse to the optical axis leads to a peak radiance (on axis) of 0.4 W/(2π sr mm^2) in 0.1% BW or 5.6×10^9 photons/(s mrad^2 mm^2 0.1% BW) spectral brightness at 1.5 kHz source repetition rate. Due to the Lorentzian shape, the emission distribution exhibits nonnegligible radial wings. The calculation based on the Cittert-Zernike theorem showed that these wings reduce significantly the illumination spatial coherence at the sample position. Therefore, a 500 µm aperture was positioned downstream (see Figure 2A, P1) of the source to crop the radiation from these wings. It resulted in the spatial coherence of about $w_{coh} = 10$ µm at the sample plane, which is comparable to the size of the illumination spot.

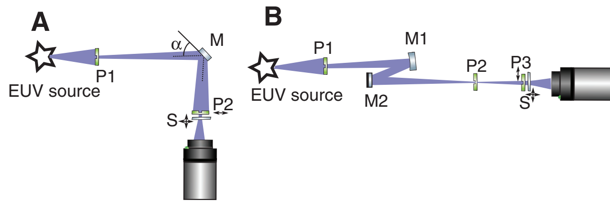

Figure 2: (A) Setup for gas discharge-based experiment with oxygen emission. P1, 500 µm diameter pinhole; P2, 10 µm pinhole; S, holey silicon nitride membrane substrate with the aluminium foil; M, a multilayer mirror for 17.3 nm central wavelength at $\alpha=43°$. The distance between the EUV source and P1 is 43 cm and that between P1 and P2 is 137 cm. (B) Setup for tin discharge-based experiments. P1, 500 µm pinhole for stray light reduction; M1 and M2, multilayer mirrors, where M2 is curved ($R=500$ mm). Close to the pinch image position, a pinhole P2 is added to adjust the coherence and to further block stray light. The pinch is demagnified by a factor of 3.6. P3, illumination pinhole of 5 µm, 40 cm separated from the pinch image; S, sample with PMMA spheres on top of a silicon nitride membrane.

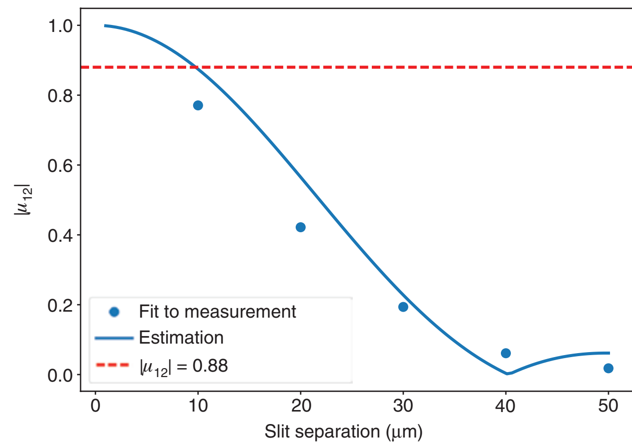

Figure 3: Results of a Young's double-slit experiment with EUV radiation from oxygen plasma (setup in Figure 2A) with a multilayer mirror but without UV/VIS filter. On the ordinate axis, the modulus of the normalized coherence factor $|\mu_{12}|$ is noted. The dots show the fitting results to the double-slit diffraction patterns for different slit separations under consideration of all emission lines within mirror bandwidth using the weighted sum of interference patterns. The residual (satellite) emission lines as well as (not accounted for) the VUV/UV/VIS background from the plasma may have led to the discrepancy between the measurement and the single-wavelength estimation shown by the solid blue line. This line shows a calculation based on the Cittert-Zernike theorem for monochromatic illumination from a Lorentzian emission source with cropped tails. The red dashed line indicates $|\mu_{12}|=0.88$, which is assumed to be the coherence limit for CDI reconstructions [28].

This was verified by a Young's double-slit experiment, the results of which are shown in Figure 3. The double-slit array (allowing different slit separations during a single exposure) was illuminated from a similar source-sample distance as that used in the ptychography experiment. The modulus of the normalized coherence factor $|\mu_{12}|$ was then determined by fitting the double-slit formula [29] to the recorded interference pattern. The details of the measurement can be found elsewhere [24]. Figure 2A shows the first ptychography setup. In addition to the blocking of the EUV emission wings, the pinhole (P1) served as a spatial coherence filter for the residual visible and UV light. Scattered from the sample, this light generates a residual, coherent background on the detector, which can be accounted for during the reconstruction by our algorithm [23]. This makes it possible to avoid UV/VIS light absorbing filters that cause high losses of the EUV radiation. Besides suppressing the coherent illumination of satellite emission lines, the multilayer mirror (M) absorbs also the short-wavelength radiation of O^{6+} at 2.16 nm, which can otherwise also create an incoherent background on the detector [30].

A 10 µm high-precision pinhole (P2; Edmund Optics) placed upstream of the sample forms a structured illumination probe on the sample. The sample to pinhole separation was roughly set to a distance below 200 µm. This was sufficient for our experiment, although for higher resolution the sample to pinhole distance would need to be further reduced to satisfy the Nyquist sampling conditions at the detector. The precise value of the working distance was obtained from the reconstruction of the illumination probe by back-propagation to a distance where the sharpest pinhole image is achieved. For sample and aperture movement, six high-precision, closed-loop translation piezo stages (Smaract SLC-1730) were used.

First, we scanned the edge of a 200 nm thick aluminium filter (Lebow Co.) placed on a holey silicon nitride membrane. This region was chosen such that both (uncovered and covered) parts of the membrane were within one reconstruction field. We have acquired diffraction patterns at 50 scanning positions, each with 60 s maximum exposure time. The dynamic range of our CCD camera was extended by stitching three different exposure times {high dynamic range (HDR) imaging [31]}. The CCD sensor (Andor iKon-M, 1024×1024 pixel, 13 µm pixel size) was cooled down to −60°C. To reach close to single-photon counting precision, a pixel readout rate of 50 kHz was used and a measured dark current background was subtracted for each pixel. Additionally, only the central region with significant photon counts was acquired to reduce the acquisition time.

The second experiment was performed using a tin plasma EUV source developed by USHIO, Inc. It is based on a laser-triggered discharge between two rotating, liquid-tin-covered disc electrodes. Detailed information about source operation and performance can be found elsewhere [32]. The source is limited to the use of tin as active medium. Tin plasma provides intensive, quasi-continuous radiation at about 13.5 nm (see Figure 1B). The source was operated at 36 W/(2π sr mm²) radiance in 2% BW (with a pinch FWHM of about 250 µm) or corresponding spectral brightness of 3.9×10^{11} photons/(s mrad² mm² 2% BW). This brightness value includes the absorption by a debris shield, which protects optics and electronics from tin contamination. The emission spectrum of tin was spectrally and spatially filtered by a system of two Mo/Si mirrors (M1 and M2) and a 200 nm thick zirconium foil in a squared window with 500 µm side length (see Figure 2B, P1). A similar design has been described in detail in Ref. [33]. The peak transmission of the filtering system was 5% with a bandwidth of about 2% at 13.5 nm of the filtered tin emission spectrum (see Figure 1B). The spatial coherence is optimized by the pinhole P2; however, due to technical constraints of the light source, the pinch imaging tool, and the experimental chamber, the spatial coherence at the sample position was better than required (estimated to be $l_{coh}>20$ µm), resulting in an ineffective use of the

available photon flux. The same pinhole reduces also the stray EUV light due to the reflections from the inner walls of the vacuum pipes.

The scanned sample (S) was placed 395 µm downstream of the structured illumination forming precision pinhole (P3) of 5 µm diameter. The sample consisted of a silicon wafer with a 200 nm thick silicon nitride window in a squared window with 500 µm side length (Norcada, Inc.) with sparsely distributed poly(methyl methacrylate) (PMMA) spheres with diameters of about 450 nm. The spheres were deposited by diluting them into a 1:1 isopropanol and water solution, spin-coating them onto the membrane, and evaporating the remaining solution [34]. At each scanning position, one HDR image was collected using a maximum of 30 s exposure time, allowing a dynamic range of up to 1:10^6. In comparison to experiments with the oxygen emission line at 17.3 nm, the higher photon energy allowed to reach close to single-photon counting precision with 1 MHz readout rate.

During the scan, 200 patterns were collected in a spiral scan with an average step size of 3 µm and with a random offset of 5% of the step size to prevent periodic artifacts [35]. The scan covered a field-of-view of about 50 µm. The sample to detector distance was 4 cm, setting the diffraction-limited resolution to 60 nm.

3 Results and discussion

The ptychography reconstruction was performed by the ePIE method [36] combined with the orthogonal probe relaxation extension (OPRP) [37]. OPRP served mainly for intensity corrections and compensation of small position errors. Otherwise, no changes in the illumination wavefront were observed thanks to the very stable illumination source. The unremoved VUV/UV/VIS background and coherence properties (spatial and temporal) of the illumination were included into the reconstruction by the generalized modulus constraint, as described in detail elsewhere [23]. Additionally, as the HDR stitched data quality depends on the level of saturation of the detector, we have accounted for the variable quality by the additional modification of the ptychography modulus constraint:

$$P_m\Psi = \left[W + (1-W)\frac{\sqrt{I}}{|\Psi|}\right]\Psi,$$

where Ψ is the original wavefront at the detector plane and $\sqrt{I}$ denotes the modulus of the measured diffraction intensity. The weighting W depends generally on the noise in data. We have used the following form:

$$W = \left[1 + \left(\frac{\left|\sqrt{I} - |\Psi|\right|}{\sigma}\right)^2\right]^{-1},$$

where σ denotes the expected noise level of the intensity modulus $\sqrt{I}$. This form of relaxed modulus constraint is a continuous extension of relaxation presented in Ref. [38]. If our modulus estimate $|\Psi|$ is closer to measured value $\sqrt{I}$, then the value of Ψ is not changed. Otherwise, in the case of a larger misfit, the modulus of Ψ is changed to $\sqrt{I}+\sigma$ or $\sqrt{I}-\sigma$. The error estimate σ was calculated from the Poisson noise distribution of the photon signal and the measured values of the readout and the dark noise for each pixel, including the noise resulting from the HDR stitching.

Finally, a relaxed support constraint was applied on the illumination probe to improve robustness and help the ptychography to mitigate artifacts from systematic errors. As the illumination probe was filtered by a pinhole that can be seen as a binary mask, there has to be a back-propagation distance z, where the probe will have exact binary support. This distance as well as the loose support of the probe can be estimated from an initial reconstruction. The probe constraint can be applied in the following form:

$$P = \Pi_z\{M[\Pi_{-z}(P)]\},$$

where $\prod_z$ denotes the near-field propagator to distance z, P is the illumination probe, and M denotes a loose estimation (mask) of the probe support S. S includes all points of the back-propagated probe $\prod_{-z}(P)$ with absolute values larger than half of their maximum value. The mask M was estimated to be 10% larger than S. The results do not depend strongly on the looseness of the mask, but looser mask improves convergence or generally helps with the reconstruction of periodic samples.

The results of the narrow-bandwidth GDP ptychography reconstruction are presented in Figure 4. The reconstruction shows the holey silicon nitride grid partly covered by a 200 nm aluminium foil. A pure aluminium foil of that thickness is expected to absorb only 26.5% of radiation at 17.3 nm [27]. However, according to our reconstruction, it absorbs 74.5 ± 1% of the radiation. Also, the relative phase shift of the pure aluminium foil should be 1.5 rad, whereas we have measured 0.51 ± 0.06 rad. Both these results suggest that the aluminium foil was strongly oxidized. If the aluminium was oxidized to Al_2O_3, the total oxide thickness would need to be 24.9 ± 0.2 nm according to the phase measurements, whereas the amplitude measurements would be best explained by 25.5 ± 1 nm. This rather strong oxidation was most likely caused by the exposure of the surface to fast oxygen ions produced in the plasma discharges that reacted with the aluminium foil when it was used to block visible light radiation during previous experiments with our gas-discharge EUV source.

In the experiment with the broadband, 13.5 nm illumination, we imaged a lower-contrast sample with rather sparse features. Despite a shorter illumination

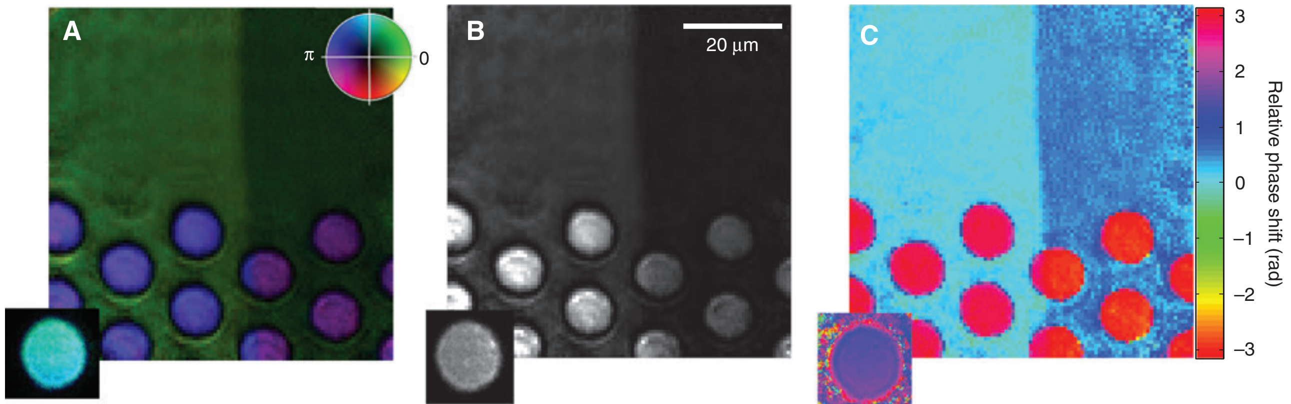

Figure 4: Reconstruction of the aluminium foil-covered holey silicon nitride membrane. The foil covers the right part of the scanned area. In contrast to our expectation, the foil absorbs most of the light, providing a strong contrast in amplitude. (A) Complex reconstruction encoded in the complex color scheme. Color represents the phase and brightness represents the amplitude. (B) Intensity-only image, showing the strong absorption introduced by the aluminium foil. (C) Phase change relative to the silicon nitride membrane. The bottom left insets contain the reconstructed illumination probe at sample plane. All images share the same scale as noted in (B).

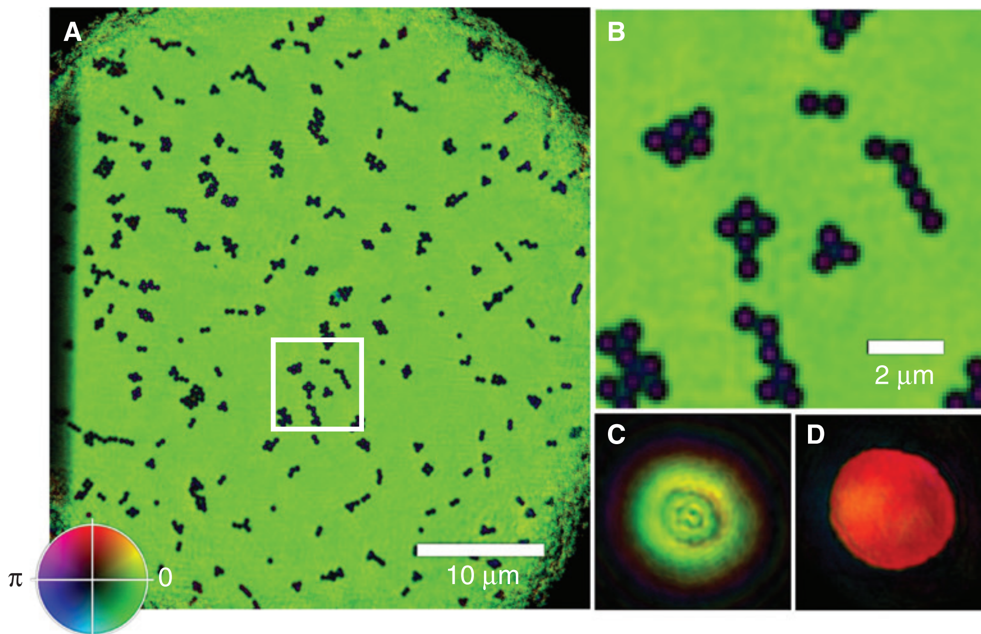

Figure 5: (A) Full-size reconstruction of the sample. PMMA spheres are clearly visible as clusters on the surface. At the left side, the edge of the membrane window is visible. (B) Zoomed version of the central region. (C) Illumination wavefront at the sample surface. It shares the same scale as in (A). The illumination spot at the substrate position already shows evolving near-field fringes. (D) Probe wavefront back-propagated to the position of the illumination forming pinhole.

wavelength and reduced scattering power of the sample, a resolution of 100 nm was achieved due to the higher photon flux of the tin-based EUV source. The reconstruction of the sample can be seen in Figure 5, whereas a scanning electron microscopy (SEM) image of a similar region of the sample is shown in Figure 6A. The SEM image contains shadows and other artifacts caused by electrostatic charging of the PMMA spheres and the dielectric substrate. EUV imaging is not accompanied by charging; therefore, it is more suitable for the quantitative analysis of the sample despite the significantly lower resolution compared to SEM images. However, the achieved resolution, depth of focus, and imaging quality are better than in images produced using visible light microscopy. A similar sample was also imaged by an EUV microscope with the high harmonic laser

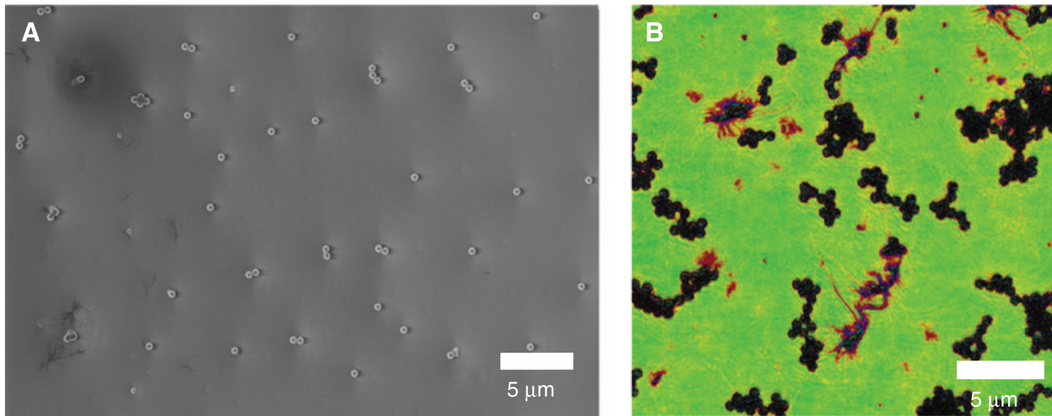

Figure 6: (A) SEM micrograph of PMMA spheres on a sample prepared similarly as the one in Figure 5. Due to charging effects, the image needed to be taken on the support frame of the membrane. (B) Ptychography reconstruction of a similar sample imaged with high harmonic laser source at 30 nm wavelength.

radiation source with 30 nm wavelength described in Ref. [39]. The difference is that the PMMA spheres were practically nontransparent binary objects (Figure 6B) at that photon energy. The imaged 450 nm PMMA should transmit more than 10% at 13.5 nm wavelength, whereas transmission at 30 nm is below 10^{-4}. In Figure 5B, one can easily see transmission in the center of the spheres, but the spheres are still surrounded by a dark ring. This ring is an artifact of the ptychography reconstruction caused by the violation of the ptychography constraints for highest spatial frequencies. Most likely, it was caused by a small amount of visible light penetrating through micropinholes in the zirconium filter and scattering from the chamber walls or stage parts producing a background at the detector. Another explanation would be the undersampling of the diffraction pattern at the detector plane due to the large distance of the illumination forming pinhole to the sample, which results in a larger than expected ring-shaped illumination spot on the sample with strong high-frequency components. Additionally, the used HDR stitching procedure could result in slightly suppressed zeroth order in the overall recorded diffraction pattern. Compared to a circle or a sphere, diffraction by a ring is characterized by a weaker zero-order maximum. Therefore, all these effects could contribute to the occurrence of the “ring artifact” in the reconstruction.

4 Summary and conclusion

In this paper, we demonstrated ptychographic imaging using EUV light from discharge plasma. We reconstructed the material composition of a thin aluminium foil EUV filter based on its complex transmission. This simple experiment would allow a quick refractive index determination of thin films with known thicknesses without complex and ambiguous fitting methods used in reflectometry measurements.

Further, we have presented for the first time ptychography with laboratory-scale tin-based plasma EUV source. We reached a resolution down to 100 nm using an illumination wavelength of 13.5 nm. This experiment proves that high-power EUV tools with tin emission spectrum can be used as a light source for ptychography.

To close the gap to real-world applications needed in applied research and industry such as lithography masks inspection, many challenges must be addressed, such as the availability of EUV sources with high brightness at 13.5 nm, limited dynamic range of detectors, and low framerate of the currently available EUV CCD cameras. Nevertheless, our experiment can already gain from an optimized mirror system, which would result in three fold reduction of exposure time. Furthermore, the tin plasma source was, due to some external constraints, only run at a quarter of its power.

Despite recent demonstration of high-resolution imaging at 13.5 nm with high harmonic laser sources on a strongly scattering artificial pattern [16], (laser) plasma sources are providing a robust platform that is commonly used in industry. Particularly, emission from a tin plasma is used in the most powerful EUV sources. Our successful experiment demonstrates that this kind of sources can be used not only for lithography, microscopy, or resist studies but also for coherent diffractive imaging (CDI) applications. Compared to synchrotron facilities with 10^{20} photons/(s mrad^2 mm^2 0.1% BW) spectral brightness

[28], discharge sources have much lower brightness leading to an increase in acquisition time and reduced resolution. Nevertheless, even highly spatially coherent HHG sources deliver ~10^9 photons/(s mrad^2 mm^2 3.5% BW) [20] in the spectral harmonics between 10 and 20 nm, which is comparable to plasma sources. In contrast to HHG and synchrotron, plasma EUV sources offer the advantage of an incoherent photon emission on the order of up to a few hundred watts at 13.5 nm [32, 40, 41]. This can be a significant advantage when CDI is combined with other methods with lower demands on the illumination coherence such as scatterometry [42] or traditional dark-field or bright-field microscopy [43–45].

The requirements of HDR can be reduced if high-NA illumination is used, similar to the X-ray ptychography experiments [46]. Especially, the availability of high-NA optics based on multilayer reflective mirrors with numerical aperture of about 0.2 and working distance larger than 1 cm [47] relaxes requirements on experimental conditions.

Additionally, due to the broad angular emission distribution (high etendue) of plasma-based EUV sources and their high emission power, several metrology “beamlines” may be used/implemented simultaneously per source, allowing for parallel CDI/ptychography measurements. This is an advantage with respect to “single-beamline” synchrotron or HHG-based methods.

Acknowledgments: M.O. acknowledges financial support from the EU FP7 Erasmus Mundus Joint Doctorate Programme EXTATIC under the framework partnership agreement FPA-2012-0033. L.J. acknowledges financial support from the Helmholtz Association for a Helmholtz Professorship (Initiative and Networking Fund). The authors acknowledge Denis Rudolf for his support and for proofreading of the article, Raoul Bresenitz for his support in the preparation before and during the experiment, and Pete Baksh for his participation on the acquisition of the high harmonic datasets and for proofreading.

References

[1] H. Kinoshita, J. Vac. Sci. Technol. B 23, 2584–2588 (2005).
[2] D. Rudolf, J. Bußmann, M. Odstrčil, M. Dong, K. Bergmann, et al., Opt. Lett. 40, 2818 (2015).
[3] M. Benk, K. Bergmann, D. Schäfer and T. Wilhein, Opt. Lett. 33, 2359–2361 (2008).
[4] D. Wilson, D. Rudolf, C. Weier, R. Adam, G. Winkler, et al., Rev. Sci. Instrum. 85, 103110 (2014).
[5] M. Tryus, S. Herbert, S. Danylyuk, D. Wilson, R. Lebert, et al., Poster Presentation, International Symposium on Extreme Ultraviolet Lithography, Maastricht (2015).
[6] M. Banyay, L. Juschkin, E. Bersch, D. Franca, M. Liehr, et al., J. Vac. Sci. Technol. A 30, 41506 (2012).
[7] S. Danylyuk, S. Herbert, P. Loosen, R. Lebert, A. Schäfer, et al., Phys. Stat. Solidi 12, 318–322 (2015).
[8] O. Maryasov, L. Juschkin, in JARA-Fit Annual Report 2015, 147–148 (2016).
[9] C. Schmitz, D. Wilson, D. Rudolf, C. Wiemann, L. Plucinski, et al., Appl. Phys. Lett, 108, 234101 (2016).
[10] S. Brose, J. Tempeler, S. Danylyuk, P. Loosen and L. Juschkin, J. Micro-Nanolitho MEM 15, 43502 (2016).
[11] E. te Sligte, N. Koster, F. Molkenboer and A. Deutz, in ‘Proc. SPIE’, 99840R (2016).
[12] J. Miao, D. Sayre and H. N. Chapman, J. Opt. Soc. Am. A 15, 1662 (1998).
[13] J. M. Rodenburg and H. M. L. Faulkner, Appl. Phys. Lett. 85, 4795 (2004).
[14] P. Thibault, M. Dierolf, O. Bunk, A. Menzel and F. Pfeiffer, Ultramicroscopy 109, 338–43 (2009).
[15] J. Miao, T. Ishikawa, I. K. Robinson and M. M. Murnane, Science 348, 530–535 (2015).
[16] F. Gardner, M. Tanksalvala, E. R. Shanblatt, X. Zhang, B. R. Galloway, et al., Nat. Photon. 11, 259 (2017).
[17] M. Holler, M. Guizar-Sicairos, E. H. Tsai, R. Dinapoli, E. Muller, et al., Nature 543, 402–406 (2017).
[18] D. J. Batey, D. Claus and J. M. Rodenburg, Ultramicroscopy 138, 13 (2014).
[19] B. Zhang, D. F. Gardner, M. H. Seaberg, E. R. Shanblatt, C. L. Porter, et al., Opt. Express 24, 18745 (2016).
[20] B. Abbey, L. W. Whitehead, H. M. Quiney, D. J. Vine, G. A. Cadenazzi, et al., Nat. Photonics 5, 420 (2011).
[21] T. Harada, H. Hashimoto, T. Amano, H. Kinoshita and T. Watanabe, J. Micro-Nanolitho MEM 15, 21007 (2016).
[22] I. Mochi, P. Helfenstein, I. Mohacsi, R. Rajeev, D. Kazazis, et al., J. Micro-Nanolitho MEM 16, 41003 (2017).
[23] M. Odstrcil, J. Bussmann, D. Rudolf, R. Bresenitz, J. Miao, et al., Opt. Lett. 40, 5574 (2015).
[24] J. Bußmann, M. Odstrčil, R. Bresenitz, D. Rudolf, J. Miao, et al., in ‘Proc. SPIE’ 95890L (2015).
[25] K. Bergmann, G. Schriever, O. Rosier, M. Müller, W. Neff, et al., Appl. Opt. 38, 5413 (1999).
[26] M. Benk, D. Schäfer, T. Wilhein and K. Bergmann, J. Phys. Conf. Ser. 186, 12024 (2009).
[27] B. L. Henke, E. M. Gullikson and J. C. Davis, At. Data Nucl. Data Tables 54, 181–342 (1993).
[28] D. Attwood, A. Sakdinawat, ‘Soft-X ray and Extreme Ultraviolet Radiation’, (Cambridge University Press, Cambridge, 2017).
[29] D. Paterson, B. E. Allman, P. J. McMahon, J. Lin, N. Moldovan, et al., Opt. Commun. 195, 79–84 (2001).
[30] L. Juschkin, L. Loetgering, D. Rudolf, R. Xu, S. Brose, et al., in ‘Proc. SPIE’, 88490Y (2013).
[31] M. Odstrcil, Doctoral dissertation, University of Southampton (2017).
[32] Y. Teramoto, B. Santos, G. Mertens, R. Kops, M. Kops, et al., in ‘Proc. SPIE’, 94220F (2015).
[33] T. Missalla, M. C. Schuermann, R. Lebert, C. Wies, L. Juschkin, et al., in ‘Proc. SPIE’, 5037 (2004).
[34] P. Baksh, Doctoral Dissertation, University of Southampton (2016).
[35] X. Huang, H. Yan, R. Harder, Y. Hwu, I. K. Robinson, et al., Opt. Express 22, 12634–44 (2014).

[36] A. M. Maiden, J. M. Rodenburg, Ultramicroscopy 109, 1256–1262 (2009).
[37] M. Odstrcil, P. Baksh, S. A. Boden, R. Card, J. E. Chad, et al., Opt. Express 24, 8360 (2016).
[38] H. N. Chapman, A. Barty, S. Marchesini, A. Noy, S. P. Hau-Riege, et al., J. Opt. Soc. Am. A 23, 1179 (2006).
[39] P. D. Baksh, M. Odstrčil, H.-S. Kim, S. A. Boden, J. G. Frey, et al., Opt. Lett. 41, 1317 (2016).
[40] M. Benk and K. Bergmann, J. Micro-Nanolitho MEM 11, 21106–1 (2012).
[41] I. Fomenkov, D. Brandt, A. Ershov, A. Schafgans, Y. Tao, et al., Adv. Opt. Technol. 6, 89–102 (2017).
[42] C. Laubis, A. Barboutis, C. Buchholz, A. Fischer, A. Haase, et al., in 'Proc. SPIE', 977627 (2016).
[43] L. Juschkin, R. Freiberger, K. Bergmann, J. Phys. Conf. Ser. 186, 12030 (2009).
[44] R. Freiberger, J. Hauck, M. Reininghaus, D. Wortmann and L. Juschkin, in 'Proc. SPIE', 80760K (2011).
[45] A. Torrisi, P. Wachulak, Ł. Węgrzyński, T. Fok, A. Bartni, et al., J. Microsc. 265, 251–260 (2017).
[46] M. Guizar-Sicairos, M. Holler, A. Diaz, J. Vila-Comamala, O. Bunk, et al., Phys. Rev. B 86, 100103 (2012).
[47] J. Ewald, M. Wieland, T. Nisius, L. Henning, T. Feigl, et al., J. Phys. Conf. Ser. 499, 12008 (2014).